Pharmaceutical Sciences and Drug Design
ISSN: 3062-4428
2024, Volume 4, Page No: 51-62

Available online at: www.galaxypub.co/page/journals

Galaxy Publication

Selective Targeting of WNK Kinases: High-Throughput Screening and Structural Insights into Isoform Specificity

Jacob Rivera[1]*, Ethan Carter[1]

[1]Department of Biotechnology, Faculty of Science, Seoul National University, Seoul, South Korea.

***E-mail** ✉ jacob.rivera.kr@gmail.com

Received: 17 November 2023; **Revised:** 09 January 2024; **Accepted:** 12 January 2024

ABSTRACT

WNK (With No Lysine [K]) kinases are serine/threonine kinases implicated in familial hyperkalemic hypertension (FHHt). Beyond blood pressure regulation, WNKs are emerging therapeutic targets for stroke and certain cancers, including triple-negative breast cancer and glioblastoma. In this study, we aimed to identify and characterize novel inhibitors of WNK kinases. A high-throughput screening of approximately 210,000 compounds was performed, followed by compound re-acquisition, secondary assays, commercial selectivity profiling, and crystallographic analysis to discover inhibitors with isoform-specific activity against WNK kinases. Five distinct classes of compounds were found to inhibit WNK1 kinase activity: quinoline derivatives, halo-sulfones, cyclopropane-containing thiazoles, piperazine-containing compounds, and nitrophenol-based molecules. These compounds broadly inhibit all four WNK isoforms, demonstrating strong pan-WNK selectivity. Notably, a subset of quinoline derivatives displayed isoform-selective potency, with greater inhibition of WNK3 compared to WNK1. Structural analysis of the quinoline compound SW120619 bound to WNK3's kinase domain revealed active site engagement, and comparison with WNK1 provided insights into the molecular basis of isoform specificity. The identified compound classes provide promising scaffolds for the development of pharmacological tools and potential therapeutic agents targeting hypertension and cancer.

Keywords: WNK, Kinase inhibitor, High-throughput screening, WNK3-selective, Structure–activity relationship, Crystallography

How to Cite This Article: Rivera J, Carter E. Selective Targeting of WNK Kinases: High-Throughput Screening and Structural Insights into Isoform Specificity. Pharm Sci Drug Des. 2024;4:51-62. https://doi.org/10.51847/ilB2Ak8vDC

Introduction

WNK (With No Lysine [K]) kinases are cytoplasmic serine/threonine protein kinases distinguished by their unique arrangement of catalytic residues [1]. They play critical roles in transepithelial ion transport, regulation of cell volume, and cell motility [2–5], establishing them as promising therapeutic targets for multiple diseases. WNK1 and WNK4 are linked to familial hyperkalemic hypertension (FHHt), also known as Gordon Syndrome [6–8], while knockout or knockdown of WNK1 and WNK3 reduces blood pressure [9, 10], supporting their relevance for hypertension treatment. Additionally, WNK kinases are implicated in cancers including breast, lung, ovarian, and brain malignancies [11–14]. Notably, transposon-based studies identify WNK1 as a proto-oncogenic signature gene in triple-negative breast cancer [15], while WNK3 knockout mice display reduced edema in stroke models [16, 17] and show overexpression in the hippocampus in certain epileptic conditions [18].

Targeting WNK kinases with small-molecule inhibitors can elucidate their biological roles and serve as starting points for drug development. Previous efforts have yielded pan-WNK inhibitors such as WNK463, which is ATP-competitive [19, 20], and allosteric inhibitors like WNK476 that bind adjacent to helix C [21]. Here, we describe novel scaffolds that selectively inhibit WNK1 and WNK3, and crystallographic analysis of a WNK3-specific inhibitor provides insights into the structural basis of isoform selectivity.

Materials and Methods

Reagents

Kinase-Glo® luminescence reagent was purchased from Promega Inc. A plasmid encoding a GST-tagged OSR1 substrate peptide (GST-TEV-GAM314RAKKVRRVPGSSGRLHKTEDGGWEWSDDEF344) was kindly provided by Melanie Cobb (UT Southwestern Medical Center, unpublished) and validated by sequencing and tandem mass spectrometry. WNK1 inhibitors identified from the screen were obtained from ChemBridge, ChemDiv, ComGenex, Prestwick, Collaborative Drug Discovery, and UT Southwestern synthesis labs. Recombinant WNK1 (residues 1–491) and WNK3 (1–431) for mobility shift assays were obtained from Carna Biosciences USA. Fluorescein-labeled OSR1 peptide (FAM-RVPGSSGRLHK-NH2) was purchased from Bachem America.

Protein expression and purification

The pWNK1 kinase domain (residues 194–483) was expressed in *E. coli* following the protocol of Min *et al*. [22], with benzonase and protease inhibitors added during lysis. Approximately 800 mg of purified protein was obtained from 25 preparations, with phosphorylation at Ser382 confirmed by mass spectrometry. A codon-optimized pWNK3 (118–409) construct was expressed and purified using the same method, with Ser308 phosphorylation verified [23]. GST-OSR1 (314–344) peptide was expressed in Rosetta (DE3) pLysS *E. coli* and purified with glutathione beads, yielding 3 g of substrate for screening.

High-throughput screening

A total of 210,000 compounds were screened in 384-well plates using the Kinase-Glo® assay (Promega) at the UT Southwestern HTS Core. Each well contained substrate solution (55.3 mM HEPES pH 7.4, 55.3 mM $MgCl_2$, 4.7 µM pWNK1, 19.3 µM GST-OSR1) with 0.2 µL DMSO (negative control) or 0.5 mM compound. ATP was added to a final concentration of 21 µM, plates were incubated for 2 h at room temperature, and luminescence was read using an EnVision plate reader (PerkinElmer).

Compound library

The UT Southwestern chemical library comprises ~210,000 compounds from multiple vendors, including ChemBridge (75,000), ChemDiv (100,000), ComGenex (22,000), TimTek (1,200), Prestwick (1,100), and the NIH Clinical Collection (450). An additional 2,500 compounds were synthesized in-house. Compounds largely comply with Lipinski's rules (MW <550 Da), and the library contains ~6,500 partially purified natural product fractions from marine bacteria.

Data analysis and hit confirmation

Screening data were analyzed using Genedata Screener® v10.1. Top hits with Z-scores >3σ were rescreened for pWNK1 and pWNK3 at 6, 4, and 0.5 µM. IC50 values were further refined for the 96 most potent compounds using nine concentrations (50 nM–49.5 µM).

Mobility-Shift assays

Kinase activity was measured via phosphorylation-induced mobility shifts of FAM-OSR1 substrate peptides in 384-well plates. GST-WNK1 or GST-WNK3 (12.5 nM final) was pre-incubated with inhibitors (0.04–10 µM) before initiating reactions with 0.5 µM FAM-OSR1 peptide and 50 µM ATP. Reactions were incubated 3 h, quenched, and analyzed using a PerkinElmer LabChip® EZ reader.

Specificity screening

SW133708, SW120619, and SW182086 were evaluated against 50 kinases spanning all five classes by Eurofins Inc. at 10 µM compound concentration using MBP or native substrates.

Crystallography

WNK3-KDm/S308A was co-crystallized with SW120619. Crystals grew at 16 °C in 0.1 M Na Malonate pH 5.0, 12% PEG3350, and were cryoprotected in 20% glycerol. Diffraction data (3.1 Å) were collected at APS 19-ID. Structures were solved by molecular replacement (PDB 5DRB) and refined using REFMAC; ligand modeling was performed in Coot. Structure coordinates are deposited under PDB 8EDH.

Differential scanning fluorimetry

pWNK1 or pWNK3 (5 μM) was incubated with 0.5 mM inhibitor, 50 mM HEPES pH 7.5, 150 mM NaCl, and 5× SYPRO Orange in 25 μL wells. Temperature was ramped from 4–80 °C in 0.5 °C increments on a Bio-Rad CFX96, monitoring fluorescence in the fluorescein channel [24].

Results and Discussion

Bootstrap screens

The phosphorylated WNK1 kinase domain (pWNK1-KDm) expressed in *E. coli* was employed for inhibitor screening. A bootstrap approach was implemented to identify WNK1 inhibitors within the UT Southwestern chemical library. At the time of the screen, the only reported WNK1 inhibitor, hypericin (US Patent Application US 2008/0286809 A1, Dario Alessi), exhibited an IC50 of 200 μM. To establish a more effective positive control, a focused sub-library of 3,500 representative compounds was screened using myelin basic protein as the substrate. This small-scale screen identified SW133708 as a promising hit. Subsequent commercial specificity testing (Eurofins) confirmed that SW133708 displayed potent pan-WNK activity, inhibiting WNK1, WNK2, and WNK4 [25].

SW133708 was then applied as a reference in a slightly larger 8,000-compound screen, which identified SW137446 as a major hit. SW137446 subsequently served as the positive control in the full 210,000-compound screen. Both the 8K and 210K screens utilized a GST-fusion construct containing the pan-WNK phosphorylation site of OSR1 [26, 27]. Performing the full screen required 3 g of the OSR1 fusion peptide and 800 mg of pWNK1-KDm.

The Z′-factor for both the 8K and 210K screens was 0.91, indicating robust separation between positive and neutral controls across plates, with only seven plates falling below this threshold **(Figure 1b)**. From the 210K screen, the top 1,275 compounds exhibiting Z-scores ≥3σ were re-screened in triplicate at concentrations of 6 μM, 4 μM, and 0.5 μM **(Figures 1c and 1d)**. The Z′-factor for the 36 confirmation plates was 0.94, demonstrating excellent assay reliability. Results from the confirmation screen closely correlated with the initial HTS data, as evidenced by the diagonal pattern observed **(Figure 1c)**. Dose-dependent inhibition was further confirmed **(Figure 1d)**, reinforcing the consistency between the 210K primary screen and the confirmation screen.

Finally, 96 selected compounds were re-screened across nine concentrations to refine IC50 values against pWNK1. Representative data are presented in **Figures 2–6.**

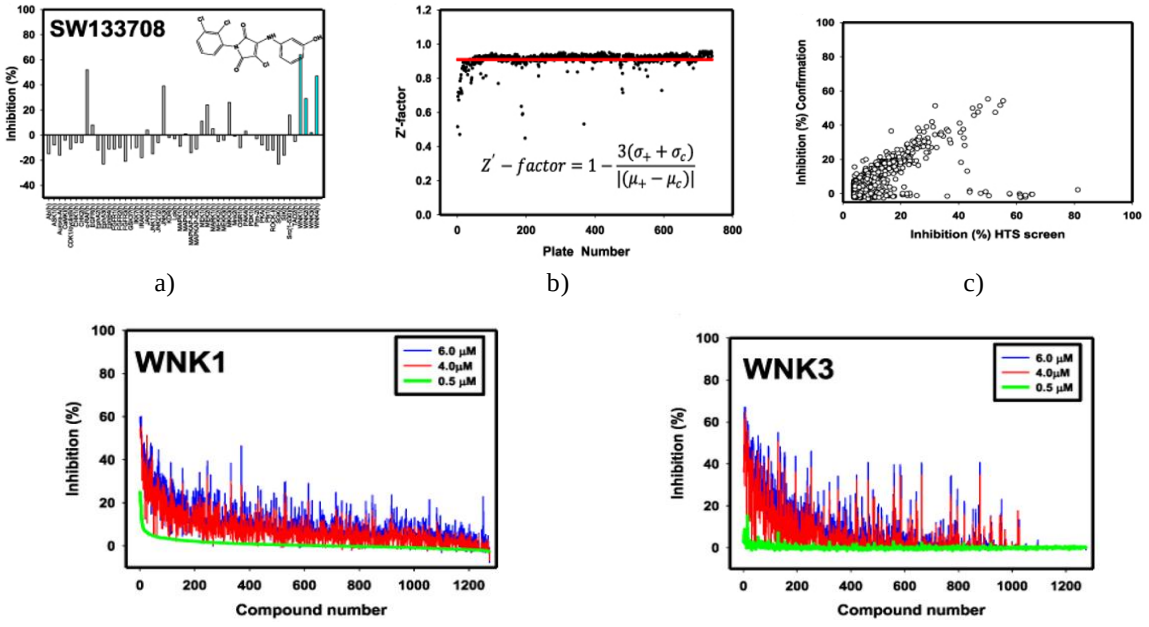

Figure 1. High-throughput and specificity screen results. (a) Commercial specificity screen (Eurofins, Inc.) testing the cross-reactivity of SW133708, the initial hit from the 3,500-compound screen, against 50 diverse kinases. (b) Z′-factor for each plate of the 210,000-compound screen (blue) is shown, with the average Z′-factor across all plates indicated by the red line. (c) Scatter plot of % inhibition in the confirmation screen

versus % inhibition in the original high-throughput screen, demonstrating consistency between screens. (d) % inhibition of each compound at 6 μM (blue), 4 μM (red), and 0.5 μM (green) toward WNK1. (e) % inhibition of each compound at the same concentrations toward WNK3.

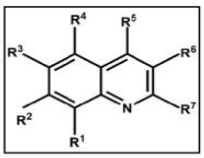

	R^1	R^2	R^3	R^4	R^5	R^6	R^7	IUPAC Name	IC_{50} WNK1 (μM)	IC_{50} WNK3 (μM)	IC_{50} WNK1* (μM)
SW120619	H	OCH_3	-	OCH_3	CH_3	H	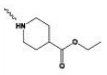	ethyl 1-(5,7-dimethoxy-4-methylquinolin-2yl)piperidine-4-carboxylate	2.3	0.7	16.8
SW120617	S-CH3	H	H	H	CH_3	H	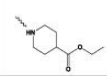	ethyl 1-(4-methyl-8-(methylthio)quinolin-2yl)piperidine-4-carboxylate	2.4	2.1	9.1
SW118150	H	OCH_3	-	OCH_3	CH_3	H	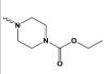	ethyl 4-(5,7-dimethoxy-4-methylquinolin-2yl)piperazine-1-carboxylate	4	1.3	16.5
SW118591	OCH_3	H	H	H	CH_3	H	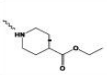	ethyl 1-(8-methoxy-4-methylquinolin-2yl)piperidine-4-carboxylate	8.2	0.7	>50
SW065844	H	H	H	H	H	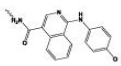	H	1-((4-methoxyphenyl)amino)-N-(quinolin-3yl)isoquinoline-4-carboxamide	1.8	3	5.8

Figure 2. Quinoline-derived inhibitors identified from the 210,000 compound screen. IC_{50} WNK1 and IC_{50} WNK3 are calculated using non-linear regression method in GraphPad from three inhibitor concentrations (6 μM, 4 μM and 0.5 μM). IC_{50}WNK1* is calculated from the refined HTS screen conducted at nine inhibitor concentrations.

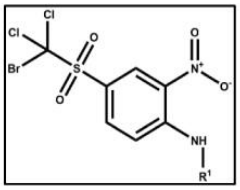

	R^1	IUPAC name	IC_{50} WNK1 (μM)	IC_{50} WNK3 (μM)	IC_{50} WNK1* (μM)
SW004355	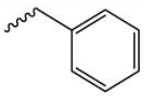	N-benzyl-4-((bromodichloromethyl) sulfonyl)-2-nitroaniline	2.9	–	–
SW004356		4-((bromodichloromethyl) sulfonyl)-Ncyclohexyl-2-nitroaniline	–	–	–
SW004357	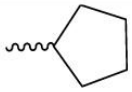	4-((bromodichloromethyl)sulfonyl)-Ncyclopentyl-2-nitroaniline	1.1	9.8	–

Figure 3. Halo-sulfone inhibitors identified from the 210,000 compound screen. IC_{50} WNK1 and IC_{50} WNK3 are calculated from three inhibitor concentrations (6 μM, 4 μM and 0.5 μM). - indicates compounds that do not meet a 3 σ criterion for the confirmation screen

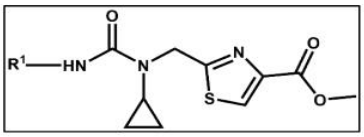

	R¹	IUPAC name	IC_{50} WNK1 (μM)	IC_{50} WNK3 (μM)	IC_{50} WNK1* (μM)
SW181808	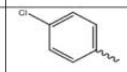	methyl 2-((3-(4-chlorophenyl)-1cyclopropylureido)methyl)thiazole-4carboxylate	48.3	-	33.05
SW181811	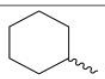	methyl 2-((3-cyclohexyl-1cyclopropylureido)methyl)thiazole-4carbo late	-	-	>50
SW181812	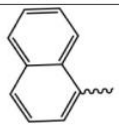	methyl 2-((1-cyclopropyl-3(naphthalen-l-yl)ureido) methyl)thiazole-4-carboxylate	-	-	>50
SW181815	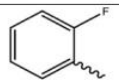	methyl 2-((1-cyclopropyl-3-(2fluorophenyl)ureido)methyl)thiazole4-carboxylate	-	-	>50
SW181816	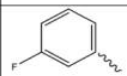	methyl 2-((l -cyclopropyl-3-(3fluorophenyl)ureido)methyl)thiazole4-carboxylate	-	-	>50
SW181817	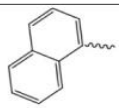	methyl 2-((1-cyclopropyl-3(naphthalen-l-yl)ureido)methyl) thiazole-4-carboxylate	-	-	>50
SW181819	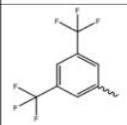	methyl 2-((3-(3,5-bis(trifluoromethyl)phenyl)-1-cyclopropylureido)methyl)thiazole-4carboxylate	-	-	>50
SW181823	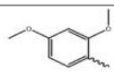	methyl 2-((1-cyclopropyl-3-(2,4dimethoxyphenyl)ureido)methyl)thiazole-4-carboxylate	4.3	1.7	16.2
SW181825	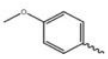	methyl 2-((1-cyclopropyl-3-(4methoxyphenyl)ureido)methyl)thiazole-4-carboxylate	9	13	17.5
SW181826	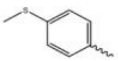	methyl 2-((1-cyclopropyl-3-(4(methylthio)phenyl)ureido)methyl) thiazole-4-carboxylate	28.1	-	19.3
SW181827	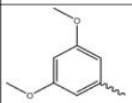	methyl 1-cyclopropyl-3-(3,5dimethoxyphenyl)ureido)methyl)thiazole-4-carboxylate	3.1	1	10.8

Figure 4. Cyclopropane-containing thiazole inhibitors identified from the 210,000 compound screen. IC_{50} WNK1 and IC_{50} WNK3 are calculated from three inhibitor concentrations (6 μM, 4 μM and 0.5 μM). IC_{50} WNK1* is calculated from the refined HTS screen conducted at nine inhibitor concentrations.

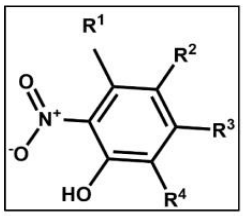

	R¹	R²	R³	R⁴	IUPAC name	IC_{50} WNK1 (μM)	IC_{50} WNK3 (μM)	IC_{50}WNK1* (μM)
SW154506	H	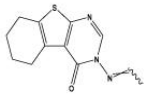	H	I	3-((4-hydroxy -3-iodo-5 -nitrobenzylidene)amino)-5,6,7 , tetrahydrobenzo [4,5]thieno[2 d]pyrimidin-4(3H)-one	8.3	-	29.5
SW053368	CH_3	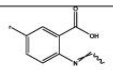	CH_3	Cl	-bromo -2-((3-chloro-6-hydro-2,4 -dimethyl-5 -nitrobenzylidene)amino)benzoic acid	3.1	-	19.8

Figure 5. Nitrophenol-derived inhibitors identified from the 210,000 compound screen. IC_{50} WNK1 and IC_{50} WNK3 are calculated from three inhibitor concentrations (6 μM, 4 μM and 0.5 μM). IC_{50} WNK1* is calculated from the refined HTS screen conducted at nine inhibitor concentrations.

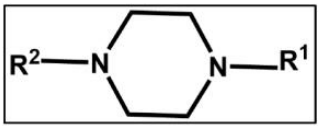

	R¹	R²	IUPAC name	IC_{50} WNK1 (μM)	IC_{50} WNK3 (μM)	IC_{50} WNK1* (μM)
SW062167	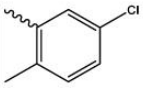	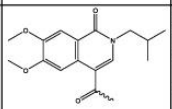	4-(4-(5-chloro-2methylphenyl)piperazine1-carbonyl)-2-isobutyl-6,7dimethoxyisoquinolin1(2H)-one	1.7	2.5	8.5
SW080005	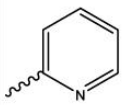	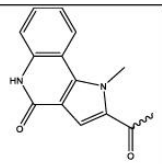	1-methyl-2-(4-(pyridin-2yl)piperazine-1-carbonyl)-1,5-dihydro-4Hpyrrolo[3,2-c]quinolin-4one	2.1	1.8	14.3

Figure 6. Piperazine-derived inhibitors identified from the 210,000 compound screen. IC_{50} WNK1 and IC_{50} WNK3 are calculated from three inhibitor concentrations (6 μM, 4 μM and 0.5 μM). $IC_{50.}$ WNK1* is calculated from the refined HTS screen conducted at nine inhibitor concentrations

Using the screening facility, the confirmation screen was cross-analyzed with phosphorylated kinase domain of WNK3 (pWNK3-KDm (pWNK3)). This screen gave similar results with respect to quality and correlation as the WNK1 screen.

Identification of compound classes

Through high-throughput screening, five distinct structural classes of WNK inhibitors were discovered: quinoline derivatives **(Figure 2)**, halo-sulfones **(Figure 3)**, cyclopropane-containing thiazoles **(Figure 4)**, piperazine derivatives **(Figure 5)**, and nitrophenol derivatives **(Figure 6).** Representative compounds from each class, along with their corresponding inhibitory potencies against pWNK1 and pWNK3, are presented in **Figures 2–6**. Notably, quinoline-derived inhibitors displayed a preference for WNK3 over WNK1, as detailed in subsequent analyses. The halo-sulfone class is described separately elsewhere [28]. The cyclopropane-thiazole series, as well as the piperazine and nitrophenol compounds, exhibited variable activity across WNK isoforms.

Selectivity assessment

Two inhibitors, SW120619 (from the quinoline class) and SW182086 (from the cyclopropane-thiazole class), were further evaluated at 10 µM for kinase selectivity against a panel of 46 protein kinases and all four WNK isoforms (Eurofins Inc., France); **(Figure 7)**. Both compounds demonstrated high specificity toward WNK kinases. Specifically, SW120619 preferentially inhibited WNK3, followed by WNK1, WNK4, and WNK2, whereas SW182086 showed comparable inhibitory activity against WNK1 and WNK3. These findings highlight the potential for developing isoform-selective WNK inhibitors.

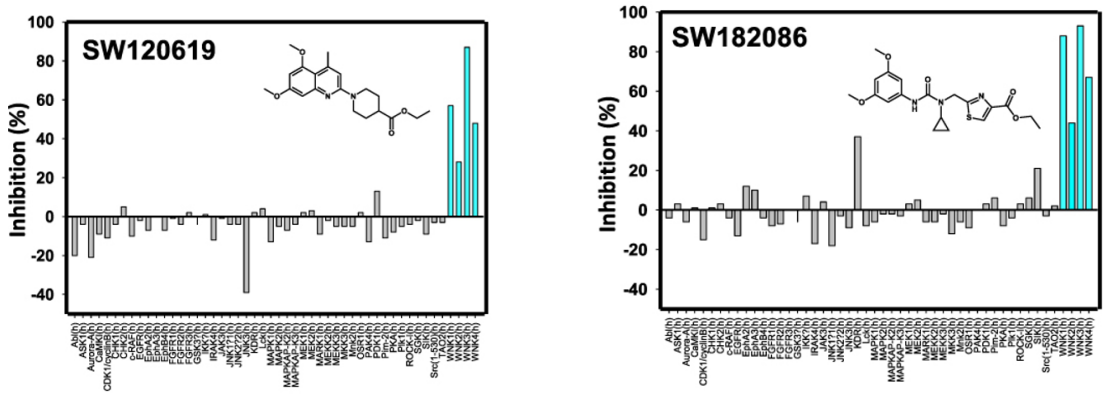

a) b)

Figure 7. Kinase selectivity assessment

The kinase selectivity of the most potent compounds from the quinoline and cyclopropane-thiazole classes was evaluated using a commercial screen (Eurofins Inc.) at a fixed concentration of 10 µM. The four human WNK isoforms are indicated by blue lines in the figure.

Quinoline class inhibitor activity

Four quinoline-derived compounds identified in the high-throughput screen were obtained from commercial vendors and tested using peptide mobility shift assays. Among these, SW120617, SW120619, and SW118150 exhibited stronger inhibition of WNK3 relative to WNK1 **(Figures 8a–8c)**. In contrast, SW118591 displayed minimal or negligible inhibitory activity against WNK3 and WNK1 **(Figure 8d)**, indicating variable potency within this chemical series.

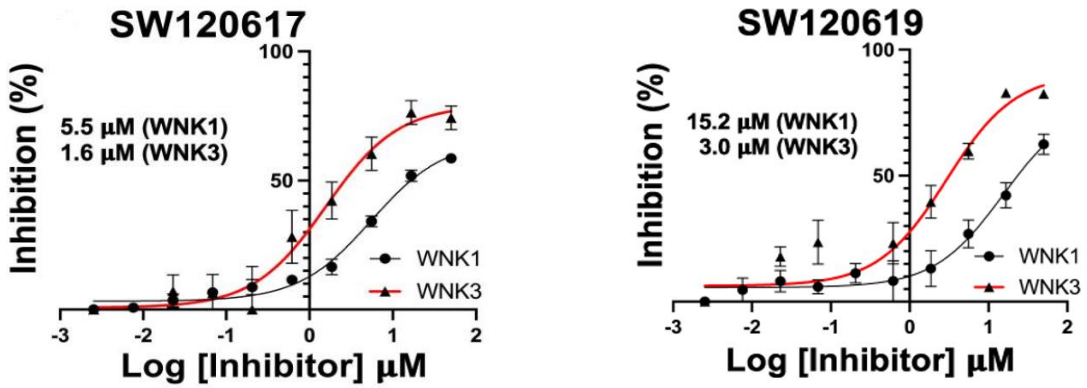

a) b)

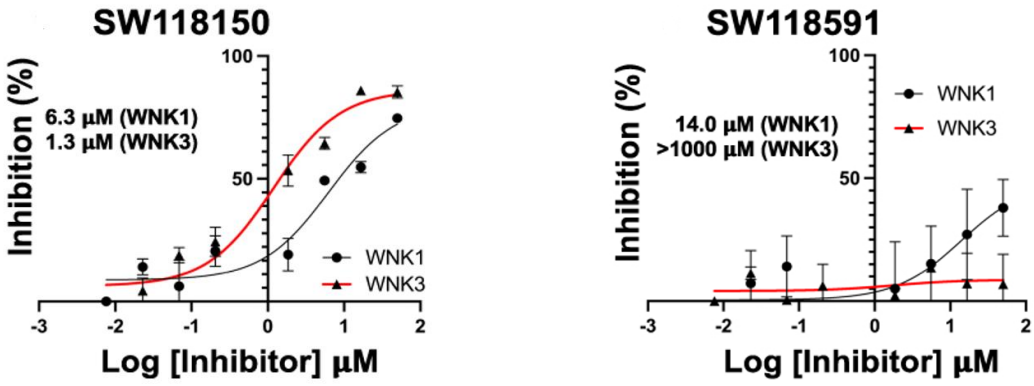

c) d)

Figure 8. Peptide mobility shift assays for quinoline class inhibitors. (a) SW120617, (b) SW120619, (c) SW118150, and (d) SW118591. GST-WNK1 (black line) and GST-WNK3 (red line) using a fluorescently labeled FAM-OXSR1 substrate peptide.

Compound characterization and specificity analysis

High-throughput screening identified five principal chemical classes that inhibit WNK kinases: quinoline derivatives, halo-sulfones, cyclopropane-containing thiazoles, piperazine derivatives, and nitrophenol-based compounds. Representative compounds from each class were selected for detailed evaluation, with their chemical structures and inhibitory activity against pWNK1 and pWNK3 presented in **Figures 2–6**. Among these, the quinoline derivatives displayed preferential inhibition of WNK3 over WNK1. The halo-sulfone series is the subject of a separate study [28]. Other compound classes included cyclopropane-thiazoles, piperazine derivatives, and nitrophenol compounds.

To determine selectivity, two inhibitors — SW120619 (quinoline class) and SW182086 (cyclopropane-thiazole class) — were tested at 10 µM against a panel of 46 kinases along with the four human WNK isoforms **(Figure 7)**. Both compounds demonstrated high selectivity toward WNK kinases. SW120619 showed a rank order of potency of WNK3 > WNK1 > WNK4 > WNK2, whereas SW182086 exhibited comparable activity against WNK1 and WNK3.

Four quinoline-class inhibitors were further examined using peptide mobility shift assays. SW120617, SW120619, and SW118150 inhibited WNK3 more strongly than WNK1 **(Figures 8a–8c)**, while SW118591 had minimal or negligible inhibitory effects on both kinases **(Figure 8d).**

Differential scanning fluorimetry (DSF) was performed to assess binding-induced thermal stabilization. All four quinoline derivatives increased the melting temperature (Tm) of both pWNK1 and pWNK3, with ΔTm values ranging from 0–2.5°C for pWNK1 and 6.5–14°C for pWNK3 **(Table 1)**, indicating stronger binding to WNK3. These thermal shifts were consistent with the IC50 data from mobility shift assays, supporting the observed isoform selectivity of these compounds.

Table 1. Change in melting temperature T_m (ΔT_m) upon binding of quinoline-derived compounds to pWNK1 and pWNK3 using differential scanning fluorimetry

Inhibitor	ΔTm pWNK1+Inhibitor (°C)	ΔTm pWNK3+Inhibitor (°C)
SW120619	2.0	7.5
SW120617	1.5	11.0
SW118150	2.5	14.0
SW118591	0.0	6.5

Crystal structure of SW120619 bound to WNK3/SA

The primary autophosphorylation site of WNK3, Ser308, was mutated to alanine (S308A) to prevent autophosphorylation, generating WNK3/SA. The X-ray structure of the WNK3/SA kinase domain in complex with the quinoline-derived inhibitor SW120619 was determined at 3.1 Å resolution by molecular replacement using the WNK1/SA structure (PDB: 6CN9) as a search model.

SW120619 (ethyl 1-(5,7-dimethoxy-4-methylquinolin-2-yl) piperidine-4-carboxylate) consists of a quinoline ring fused to a piperidine scaffold and is well-resolved in the electron density **(Figure 9a).** The inhibitor adopts an orientation roughly perpendicular to the β-strands of the N-terminal lobe, engaging two ridge-like regions of the β-sheet. On one ridge, SW120619 interacts with L153, V161, C176, and L225, while on the second ridge, it contacts A174 and T227. Additionally, it engages the backbone of residues L229–T231 located at the crossover connection between the N- and C-terminal lobes **(Figure 9b).**

On the opposite face of the kinase, SW120619 forms extensive interactions with F282 and establishes contacts with the catalytic residues K159 and D294. Its methoxy substituents interact with the chloride-binding helix (CBH) at the N-terminal region of the activation loop (previously described as the "3_{10} helix"), specifically contacting the main chain of L295 and the side chain of L297 **(Figure 9b).**

Structurally, SW120619 resembles the pan-WNK inhibitor WNK463 reported by Novartis, both in overall molecular architecture and binding orientation **(Figure 9c)**. Like WNK463, SW120619 consists of a linear arrangement of heterocyclic rings and occupies the same binding pocket near the crossover connection. However, SW120619 does not extend as deeply into the active site as WNK463.

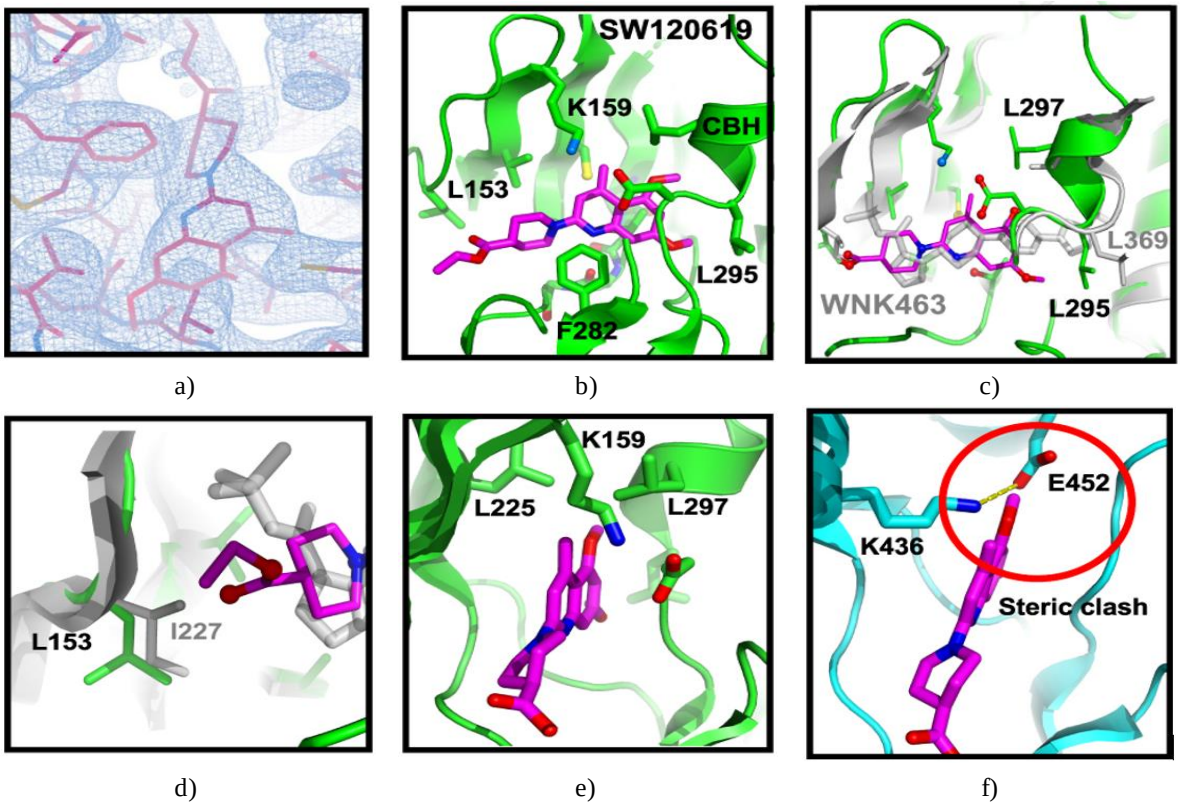

Figure 9. Structure of complex between WNK3/SA and SW120619. (a) Electron density of the inhibitor SW120619 contoured at 0.5 σ. (b) Schematic of the inhibitor binding drawn in Pymol (c) Superposition of WNK3/SW120619 with WNK1/6CN9. The superposition encompassed residues forming the binding site, WNK1/225–236, 298–308, 353-375 (in WNK3, WNK3/151-162, 223–233, 279-301) (d) Closeup of SW120619 and WNK463 near L153 in WNK3 (I227 in WNK1). (e) The WNK3/SW120619 complex oriented to highlight the differences between WNKs and more standard protein kinases such as PAK6 (PDB file 2C30). (f) PAK6 oriented in comparison with (e). Red circle indicates steric clash between SW120619 and PAK6.

Structural basis for WNK3 selectivity of SW120619

Comparison of WNK3 and WNK1 residues contacting SW120619 revealed a single amino acid difference, with leucine at position 153 in WNK3 corresponding to isoleucine 227 in WNK1 **(Figure 9d)**. This substitution, combined with the specific binding orientation of SW120619, likely contributes to the observed WNK3 selectivity. To further evaluate the binding mode, the WNK1 structure complexed with WNK463 was locally superimposed onto WNK3/SW120619 using secondary structure elements that define the inhibitor binding site

(Figure 9c). The superposition shows that SW120619 makes direct contact with WNK3/L153, whereas WNK463 does not **(Figure 9d)**. Additional subtle variations in the chloride-binding helix (CBH), including L295 and L297 in WNK3, may also underlie the selective binding of SW120619.

The enhanced potency of quinoline-derived inhibitors toward WNK3 suggests the feasibility of developing isoform-specific compounds. Analysis of the WNK3/SW120619 structure compared with canonical serine/threonine kinases, such as PAK6, indicates that the inhibitor occupies a pocket that is sterically incompatible with standard kinase structures **(Figures 9e–9f)**. In WNK3, the pocket accommodating the quinoline moiety is accessible due to the unique positioning of residues and the absence of a steric clash seen in PAK6. These observations rationalize both the pan-WNK activity and the potential for isoform selectivity of quinoline-based inhibitors.

Crystallographic data indicate that SW120619 occupies the same pockets as the pan-WNK inhibitor WNK463 but engages a smaller subset of binding sites (Pockets I and II). Modeling of other quinoline analogues highlights potential positions for chemical modification, supporting rational design approaches to enhance isoform specificity. This structural insight provides a foundation for the development of selective WNK1 or WNK3 inhibitors.

Conclusion

Through high-throughput screening, we identified selective inhibitors of WNK1 and WNK3 with strong specificity toward WNK kinases over a panel of 46 other kinases. Structural comparisons between WNK isoforms and canonical serine/threonine kinases reveal active site differences that account for this selectivity. Quinolinederived compounds exhibited higher potency against WNK3 compared with WNK1, and structural analysis provides guidance for designing isoform-specific inhibitors. These inhibitors serve as valuable starting points for developing pharmacological tools to investigate isoform-specific WNK functions in signal transduction and their roles in hypertension, cancer, and other diseases.

Acknowledgments: We thank Clinton Taylor and Melanie Cobb for the gOSR1 peptide. We thank Anwu Zhou for help in analyzing the HTS data. Results shown in this report were derived from work performed at Argonne National Laboratory, Structural Biology Center (SBC) at the Advanced Photon Source. The SBC is operated by the U Chicago Argonne, LLC, for the US Department of Energy, Office of Biological and Environmental Research under contract DE-AC02-06CH11357. Crystallographic studies were coordinated by Diana Tomchick in the UT Southwestern Structural Biology Laboratory. We thank Kenneth Westover for helping with the mobility-shift assays.

Conflict of Interest: None

Financial Support: This work was supported by the American Heart Association grants 16SA285300002 and 14GRNT20500035, the Welch Foundation grants I1128 and I-2100-20220331, and CPRIT grant RP190421 to EJG and a pilot grant from Harold C. Simmons Comprehensive Cancer Center to EJG and RA.

Ethics Statement: None

References

1. Xu B, English JM, Wilsbacher JL, Stippec S, Goldsmith EJ, Cobb MH. WNK1, a novel mammalian serine/threonine protein kinase lacking the catalytic lysine in subdomain II. J Biol Chem. 2000;275(22):16795–801. doi:10.1074/jbc.275.22.16795
2. Kahle KT, Rinehart J, Lifton RP. Phosphoregulation of the Na-K-2Cl and K-Cl cotransporters by the WNK kinases. Biochim Biophys Acta. 2010;1802(12):1150–8. doi:10.1016/j.bbadis.2010.07.009
3. Cruz-Rangel S, Gamba G, Ramos-Mandujano G, Pasantes-Morales H. Influence of WNK3 on intracellular chloride concentration and volume regulation in HEK293 cells. Pflugers Arch. 2012;464(3):317–30. doi:10.1007/s00424-012-1137-4

4. Choe KP, Strange K. Evolutionarily conserved WNK and Ste20 kinases are essential for acute volume recovery and survival after hypertonic shrinkage in Caenorhabditis elegans. Am J Physiol Cell Physiol. 2007;293(3):915–27. doi:10.1152/ajpcell.00126.2007
5. Tu SW, Bugde A, Luby-Phelps K, Cobb MH. WNK1 is required for mitosis and abscission. Proc Natl Acad Sci U S A. 2011;108(4):1385–90. doi:10.1073/pnas.1018567108
6. Wilson FH, Disse-Nicodème S, Choate KA, Ishikawa K, Nelson-Williams C, Desitter I, et al. Human hypertension caused by mutations in WNK kinases. Science. 2001;293(5532):1107-12. doi:10.1126/science.1062844
7. Tobin MD, Raleigh SM, Newhouse S, Braund P, Bodycote C, Ogleby J, et al. Association of WNK1 gene polymorphisms and haplotypes with ambulatory blood pressure in the general population. Circulation. 2005;112(22):3423-9. doi:10.1161/CIRCULATIONAHA.105.555474
8. Dbouk HA, Huang CL, Cobb MH. Hypertension: the missing WNKs. Am J Physiol Renal Physiol. 2016;311(1):F16–F27. doi:10.1152/ajprenal.00358.2015
9. Zambrowicz BP, Abuin A, Ramirez-Solis R, Richter LJ, Piggott J, BeltrandelRio H, et al. Wnk1 kinase deficiency lowers blood pressure in mice: a gene-trap screen to identify potential targets for therapeutic intervention. Proc Natl Acad Sci U S A. 2003;100(24):14109-14. doi:10.1073/pnas.2336103100
10. Oi K, Sohara E, Rai T, Misawa M, Chiga M, Alessi DR, et al. A minor role of WNK3 in regulating phosphorylation of renal NKCC2 and NCC co-transporters in vivo. Biol Open. 2012;1(2):120-7. doi:10.1242/bio.2011048. Epub 2011 Nov 24.
11. Davies H, Hunter C, Smith R, Stephens P, Greenman C, Bignell G, et al. Somatic mutations of the protein kinase gene family in human lung cancer. Cancer Res. 2005;65(17):7591-5. doi:10.1158/0008-5472
12. Jinawath N, Vasoontara C, Jinawath A, Fang X, Zhao K, Yap KL, et al. Oncoproteomic analysis reveals co-upregulation of RELA and STAT5 in carboplatin resistant ovarian carcinoma. PLoS One. 2010 ;5(6):e11198. doi:10.1371/journal.pone.0011198
13. Zhu W, Begum G, Pointer K, Clark PA, Yang SS, Lin SH, et al. WNK1-OSR1 kinase-mediated phospho-activation of Na+-K+-2Cl- cotransporter facilitates glioma migration. Mol Cancer. 2014;13:31. doi:10.1186/1476-4598-13-31
14. Xie T, D' Ario G, Lamb JR, Martin E, Wang K, Tejpar S, et al. A comprehensive characterization of genome-wide copy number aberrations in colorectal cancer reveals novel oncogenes and patterns of alterations. PLoS One. 2012;7(7):e42001. doi:10.1371/journal.pone.0042001
15. Chen L, Jenjaroenpun P, Pillai AM, Ivshina AV, Ow GS, Efthimios M, et al. Transposon insertional mutagenesis in mice identifies human breast cancer susceptibility genes and signatures for stratification. Proc Natl Acad Sci U S A. 2017;114(11):E2215-E2224. doi:10.1073/pnas.1701512114
16. Begum G, Yuan H, Kahle KT, Li L, Wang S, Shi Y, et al. Inhibition of WNK3 kinase signaling reduces brain damage and accelerates neurological recovery after stroke. Stroke. 2015;46(7):1956-65. doi:10.1161/STROKEAHA.115.008939
17. Zhao H, Nepomuceno R, Gao X, Foley LM, Wang S, Begum G, et al. Deletion of the WNK3-SPAK kinase complex in mice improves radiographic and clinical outcomes in malignant cerebral edema after ischemic stroke. J Cereb Blood Flow Metab. 2017;37(2):550-63. doi:10.1177/0271678X16631561
18. Jeong KH, Kim SH, Choi YH, Cho I, Kim WJ. Increased expression of WNK3 in dispersed granule cells in hippocampal sclerosis of mesial temporal lobe epilepsy patients. Epilepsy Res. 2018;147:58–61. doi:10.1016/j.eplepsyres.2018.09.006
19. Yamada K, Park HM, Rigel DF, DiPetrillo K, Whalen EJ, Anisowicz A, et al. Small-molecule WNK inhibition regulates cardiovascular and renal function. Nat Chem Biol. 2016;12(11):896-8. doi:10.1038/nchembio.2168
20. Yamada K, Levell J, Yoon T, Kohls D, Yowe D, Rigel DF, et al. Optimization of allosteric With-No-Lysine (WNK) kinase inhibitors and efficacy in rodent hypertension models. J Med Chem. 2017;60(16):7099-107. doi:10.1021/acs.jmedchem.7b00708
21. Yamada K, Zhang JH, Xie X, Reinhardt J, Xie AQ, LaSala D, et al. Discovery and characterization of allosteric WNK kinase inhibitors. ACS Chem Biol. 2016;11(12):3338-46. doi:10.1021/acschembio.6b00511
22. Min XS, Lee BH, Cobb MH, Goldsmith EJ. Crystal structure of the kinase domain of WNK1, a kinase that causes a hereditary form of hypertension. Structure. 2004;12(7):1303–11. doi:10.1016/j.str.2004.04.014

23. Akella R, Humphreys JM, Sekulski K, He H, Durbacz M, Chakravarthy S, et al. Osmosensing by WNK kinases. Mol Biol Cell. 2021;32(18):1614-23. doi:10.1091/mbc.E20-01-0089
24. Manning G, Whyte DB, Martinez R, Hunter T, Sudarsanam S. The protein kinase complement of the human genome. Science. 2002;298(5600):1912–34. doi:10.1126/science.1075762
25. Pantoliano MW, Petrella EC, Kwasnoski JD, Lobanov VS, Myslik J, Graf E, et al. High-density miniaturized thermal shift assays as a general strategy for drug discovery. J Biomol Screen. 2001;6(6):429-40. doi:10.1177/108705710100600609
26. Anselmo AN, Earnest S, Chen W, Juang YC, Kim SC, Zhao Y, et al. WNK1 and OSR1 regulate the Na+, K+, 2Cl- cotransporter in HeLa cells. Proc Natl Acad Sci U S A. 2006;103(29):10883-8. doi:10.1073/pnas.0604607103. Epub 2006 Jul 10
27. Vitari AC, Thastrup J, Rafiqi FH, Deak M, Morrice NA, Karlsson HK, et al. Functional interactions of the SPAK/OSR1 kinases with their upstream activator WNK1 and downstream substrate NKCC1. Biochem J. 2006;397(1):223-31. doi:10.1042/BJ20060220
28. Rodriguez M, Kannangara A, Chlebowicz J, Akella R, He H, Tambar UK, et al. Synthesis and structural characterization of novel trihalo-sulfone inhibitors of WNK1. ACS Med Chem Lett. 2022;13(10):1678-84. doi:10.1021/acsmedchemlett.2c00216